Resonant Property Analysis of Metamaterials filled with Nonlinear Magnetic Cores

Mauro Bologna[1], Kristopher J. Chandía[1] *Member, IEEE*, and Bernardo Tellini[2] *Senior Member, IEEE*
[1]Departamento de Ingeniería Eléctrica-Electrónica, Universidad de Tarapacá, Arica, Chile
[2]Dipartimento di Ingegneria dell'Energia, dei Sistemi, del Territorio e delle Costruzioni, Universita di Pisa, Largo Lucio Lazzarino, I-56122, Pisa, Italy

In this paper, we present a novel study on a metamaterial with nonlinear magnetic core filled-resonators. We adopt an equivalent nonlinear circuit model, describing the magnetic core behavior in the Rayleigh region. We then derive the solution through perturbative analytical approaches. In particular, we show that the nonlinearity of the filling material generates secondary resonances at which the metamaterial amplifies the input field and exhibits a negative effective magnetic permeability. We validate the analytical results with numerical simulations performed via a circuit simulator. Finally, we report our discussion and conclusion.

***Index Terms*—Circuit analysis, metamaterials, nonlinear properties, perturbation analysis, resonance.**

I. Introduction

THE development and study of novel materials with new properties is a wide field of active research. Focusing on electromagnetic properties, we have the relevant work of [1] that contributes to the generation of new material with peculiar new electromagnetic properties. Starting from the original work of [1] in the microwave regime, new theoretical and experimental works have expanded the frequency range considerably that metamaterials and composite materials can operate [2], [3], [4], [5], [6], [7], [8], [9]. In particular in [10] a metamaterial absorber is designed within the visible light regime, while in [5] and in [6] the authors built structures exhibiting negative effective permeability in the kHz frequency range. Metamaterials with negative μ operating at optical frequencies can be used to design superlens, while metamaterials with negative μ at kHz and MHz frequencies may help to enhance shieldings [11] and wireless power transfer [12], as well as exhibit intrinsic stability in magnetic levitation [13], [14], thus showing the wide range of possible applications. The possibility to control the metamaterial behavior introducing nonlinear elements appears also an intriguing argument. Some studies approached this aspect using dielectric nonlinearity, mechanical and thermal effects [15], [16], [17].

Here, we study the modified structure realized in [5] filling up the resonant cavity with a hysteretical material operating in the Rayleigh region [18]. Adding ferrite to the setup of [5], we will show that, besides the principal resonance, the nonlinearity of the material generates secondary resonances. The main characteristic of the secondary resonance is a moderate amplification of the signal, giving the advantages of resonance but keeping the magnetic filling material in the Rayleigh zone. Further, being one of the two secondary resonances the half of the main resonance, this positively impacts the cell dimensions of a hypothetical metamaterial. As discussed throughout the paper, we will use a nonlinear circuital model to describe the system we are willing to study. Our effort will focus on equations such as

$$\frac{d^2x}{dt^2} + x = \varepsilon h\left(x, \frac{dx}{dt}, t\right) \tag{1}$$

To study the above equation, we will adopt two analytical procedures: the Multiple Scales [19] and the Average Theorem [20]

The paper is organized as follows: In Sec. II we present the theoretical model. In Sec. III we study the nonlinear circuit near the resonance. In Sec. IV we show, analytically, that the system has a secondary resonance. Finally in Sec. VII we draw our conclusions.

II. Model

Let us consider a metamaterial composed of an array of indefinitely long cylinders as shown in Fig. 1 (cross-section). Each grey cylinder represents a solenoid filled with a magnetic material and closed through a capacitor to form a resonator. The squares define the unit cells of the metamaterial. As demonstrated in [5], the study of the metamaterial can be reduced to the study of one unit cell inserted in an external solenoid. As a consequence, the configuration reduces to that shown in Fig. 2, through which we recognize the external solenoid (solid lines) and the resonator (dash-dotted line) with a symbol of the magnetic filling (bold lines). The two small squares represent a search coil through which we can evaluate the average magnetic flux density, while the two small circles indicate a second search coil to measure the average magnetic flux density in the region inside the external solenoid and outside the resonator. A detailed discussion of this configuration and the implemented measurement procedure to characterize a structured array of resonators via a "unit-cell" setup is available in [5], [6]. Besides, cell dimensions, main parameter values, and characteristic frequencies are discussed throughout those papers.

The equivalent circuit model of the configuration shown in Fig. 2 is reported in Fig. 3. In more detail, L_{11} and

Manuscript received December 1, 2012; revised August 26, 2015. Corresponding author: B. Tellini (email: bernardo.tellini@unipi.it).

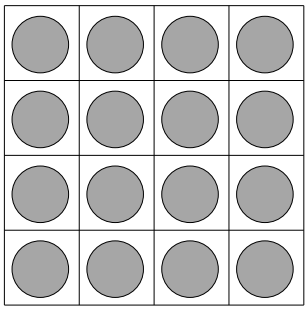

Fig. 1. Representation of the metamaterial with the array of magnetically nonlinear resonators. The square with the thicker border and a dashed motif represents the unit-cell.

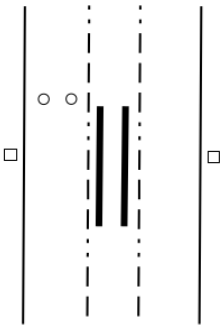

Fig. 2. Schematic section of the unit-cell with the external solenoid (solid lines), the resonator (dash-dotted line), the magnetic filling (bold lines), and the two search coils (squares and circles refer to B_{ave} and $\mu_0 H_{ave}$, respectively).

L_{22} represent the differential self inductances of the external solenoid and the resonator, respectively, while $L_{21} = L_{12} \equiv M$ stands for the differential mutual inductance between the two solenoids. The parameters R_2 and C_2 are the resistance and capacitance of the resonator circuit. The voltages v_{o3} and v_{o4} are the induced voltages along with the two search coils, small circles, and small squares, respectively, of Fig. 2. Such voltages can be measured as discussed in [5], providing the average field $\mu_0 H_{ave}$ (coil with circles) and the average magnetic flux density B_{ave} (coil with squares) over the unit-cell region.

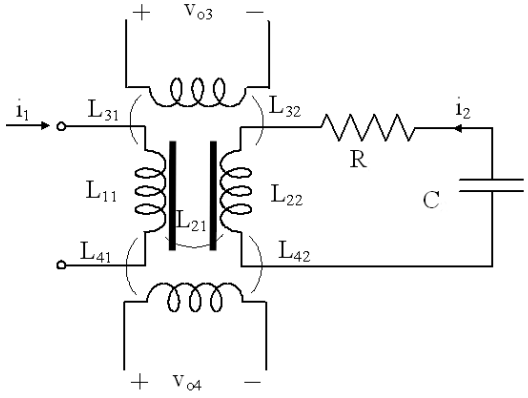

Fig. 3. Equivalent circuit of the resonant system with nonlinear inductances.

Applying Faraday-Lenz's law, knowing the magnetic flux $\Phi\left[i_1, M(i_1,i_2), i_2, L_{22}(i_1,i_2)\right]$ linked with the resonator solenoid, we have

$$V_2 = \frac{d\Phi}{dt} = \frac{\partial\Phi}{\partial i_1}\frac{di_1}{dt} + \frac{\partial\Phi}{\partial M}\frac{dM}{dt} + \frac{\partial\Phi}{\partial i_2}\frac{di_2}{dt} + \frac{\partial\Phi}{\partial L_{22}}\frac{dL_{22}}{dt}, \quad (2)$$

where V_2 is the voltage across L_{22}. Evaluating the derivatives we write

$$V_2 = \left(M + i_1\frac{\partial M}{\partial i_1} + i_2\frac{\partial L_{22}}{\partial i_1}\right)\frac{di_1}{dt} + \left(L_{22} + i_1\frac{\partial M}{\partial i_2} + i_2\frac{\partial L_{22}}{\partial i_2}\right)\frac{di_2}{dt}. \quad (3)$$

Let us assume the same turn density for the two solenoids to simplify our analysis. As a consequence, we can infer $L_{22}(i_1,i_2) = M(i_1,i_2)$, since all the linked magnetic flux with the resonator links also with the external solenoid. Expanding up to the first nonlinear term, the $B-H$ relationship of the magnetic filling material, we can write:

$$B(H) \approx aH + bH^2, \quad (4)$$

where the right-hand term is representative of the $B-H$ relationship in the Rayleigh zone.

Besides, we may associate the differential permeability $\mu \equiv \mu(H) = \partial B/\partial H$ to a differential self inductance $L_{22}(i_1+i_2)$, and $H \propto i_1 + i_2$ inside the resonator, due to the superposition of the two magnetic fields generated by i_1 and i_2. Consequently, $L_{22} = L_0 + \alpha_L(i_1+i_2)$, and analogously $M = M_0 + \alpha_M(i_1+i_2)$, where the quantities differential L_0 and M_0 are the constant terms of the self and mutual inductance, respectively. In particular, we can derive the parameters a and b through a characterization of the magnetic material sample. Then we can estimate L_0 and α considering the cell and resonator geometry. Further, we consider the case in which $i_1(t)$ is a given harmonic function, $i_1(t) = i_0\cos(\omega t + \phi_1)$ and $i_2(t) \equiv dq_2/dt$ is the current flowing in the resonator circuit. Adding a capacitor C and a resistance R, the electromotive balance equation of the resonator circuit writes as:

$$\left[M_0 + 2\alpha_M i_1 + (\alpha_M+\alpha_L)\frac{dq_2}{dt}\right]\frac{di_1}{dt} + \left[L_0 + 2\alpha_L\frac{dq_2}{dt} + (\alpha_M+\alpha_L)i_1\right]\frac{d^2q_2}{dt^2} + R\frac{dq_2}{dt} + \frac{q_2}{C} = 0 \quad (5)$$

Let us write (5) in dimensionless variable. For sake of simplicity we may set $M_0 = L_0 \equiv L$, $\alpha_M = \alpha_L \equiv \alpha$ and $dq_1/dt \equiv i_1(t)$; thus we have

$$\frac{d^2q_2}{dt^2} + \frac{R}{L\left[1 + \frac{2\alpha}{L}\left(\frac{dq_2}{dt} + \frac{dq_1}{dt}\right)\right]}\frac{dq_2}{dt} + \frac{q_2}{LC\left[1 + \frac{2\alpha}{L}\left(\frac{dq_2}{dt} + \frac{dq_1}{dt}\right)\right]} = -\frac{d^2q_1}{dt^2}. \quad (6)$$

Introducing the following notation

$$\omega_C^2 = \frac{1}{LC},\ Q = \frac{q_2}{Q_0},\ Q_1 = \frac{q_1}{Q_0},\ \varepsilon = \frac{2\alpha Q_0 \omega_C}{L}, \quad (7)$$

$$\beta = \frac{R}{2\alpha Q_0 \omega_C^2},\ T = \omega_C t,\ \tau = \varepsilon \omega_C T, \quad (8)$$

we define the parameter ε as the ratio between a reference inductance, i.e., $2\alpha Q_0 \omega_C$, proportional the nonlinearity parameter α, and the inductance L. To ensure the validity of our perturbative approach, we required that $\varepsilon \ll 1$. Similarly, β is representative of a dimensionless resistance. More in general, β is not required to be a small parameter, and for our purposes, we assume that $\varepsilon\beta$ is also a small term. We may rewrite (6) as

$$\frac{d^2Q}{dT^2} + \frac{\varepsilon\beta}{\left[1+\varepsilon\left(\frac{dQ}{dT}+\frac{dQ_1}{dT}\right)\right]}\frac{dQ}{dT} + \frac{Q}{\left[1+\varepsilon\left(\frac{dQ}{dT}+\frac{dQ_1}{dT}\right)\right]} = -\frac{d^2Q_1}{dT^2}. \quad (9)$$

For what follows, we consider a simplified expression of the above equation since we will limit our analysis to the case of $\varepsilon \ll 1$. Developing the denominator of Eq. (9) in power of ε we have, at first order,

$$\left[1+\varepsilon\left(\frac{dQ}{dT}+\frac{dQ_1}{dT}\right)\right]^{-1} \simeq 1-\varepsilon\left(\frac{dQ}{dT}+\frac{dQ_1}{dT}\right) \quad (10)$$

Plugging Eq. (10) into Eq. (9) and keeping the terms up to the first-order ε, we have

$$\frac{d^2Q}{dT^2} + Q = -\frac{d^2Q_1}{dT^2} + \varepsilon\left[-\beta\frac{dQ}{dT} + Q\left(\frac{dQ}{dT}+\frac{dQ_1}{dT}\right)\right]. \quad (11)$$

III. Solution near the primary resonance

In this section, we study the electric system near the primary resonance, i.e., when the external source is a periodic signal with a frequency $\omega \approx \omega_C$. To perform an analytical progress, we will adopt the technique of the multiple scales [19]. Near the primary resonance, we consider a weak external current $i_1(t)$ near the resonance, i.e.,

$$i_1(t) = \varepsilon i_{01} \sin[(1+\varepsilon\Omega)\omega_C t] \quad (12)$$

corresponding to the dimensionless function

$$\frac{dQ_1}{dT} = \varepsilon f \sin[(1+\varepsilon\Omega)T],\ f = \frac{i_{01}}{Q_0\omega_C} \quad (13)$$

We assume the ε expansion for (11) with the charge expansion

$$Q = \sum_{n=0}^{\infty} \varepsilon^n F_n(T^+,\tau) = F_0(T^+,\tau) + \varepsilon F_1(T^+,\tau) + \cdots \quad (14)$$

where T^+ is the strained variable of the form $T^+ = T(1+\varepsilon^2\gamma_2 + \cdots)$ with $\gamma_2, \gamma_3 \ldots$ coefficients that have to be determined. The slow variations are considered to depend on $\tau = \varepsilon T$. Up to the first-order ε, it is sufficient to consider $T^+ = T$. From (11), we have

$$\frac{d^2Q}{dT^2} + Q = \varepsilon\left[-f\cos(T+\Omega\tau) - \beta\frac{dQ}{dT} + Q\frac{dQ}{dT}\right] \quad (15)$$

Applying the multiple scale approach (see [19] for more details)

$$\frac{\partial^2}{\partial T^2}F_0(T,\tau) + F_0(T,\tau) = 0 \quad (16)$$

$$\frac{\partial^2}{\partial T^2}F_1(T,\tau) + F_1(T,\tau) = -f\cos(T+\Omega\tau) - \beta\frac{\partial}{\partial T}F_0(T,\tau) + F_0(T,\tau)\frac{\partial}{\partial T}F_0(T,\tau) + -2\frac{\partial^2}{\partial T\partial\tau}F_0(T,\tau). \quad (17)$$

We make the ansatz $F_0(T,\tau) = A(\tau)\cos(T+\Omega\tau) + B(\tau)\sin(T+\Omega\tau)$ and imposing the condition that mixed-secular terms vanish we have the following differential equation system

$$-\Omega A(\tau) + \frac{\beta}{2}B(\tau) + B'(\tau) = -\frac{f}{2}, \quad (18)$$

$$A'(\tau) + \frac{\beta}{2}A(\tau) + \Omega B(\tau) = 0. \quad (19)$$

The solution is promptly found

$$A(\tau) = e^{-\frac{1}{2}\beta\tau}\left[\left(a_0 - \frac{2f\Omega}{\beta^2+4\Omega^2}\right)\cos\Omega\tau - \frac{\beta f\sin\Omega\tau}{\beta^2+4\Omega^2}\right] + \frac{2f\Omega}{\beta^2+4\Omega^2} \quad (20)$$

$$B(\tau) = e^{-\frac{1}{2}\beta\tau}\left[\left(a_0 - \frac{2f\Omega}{\beta^2+4\Omega^2}\right)\sin\Omega\tau + \frac{\beta f\cos\Omega\tau}{\beta^2+4\Omega^2}\right] - \frac{\beta f}{\beta^2+4\Omega^2}, \quad (21)$$

in agreement with [19]. The solution is

$$Q(T) = A(\tau)\cos(T+\Omega\tau) + B(\tau)\sin(T+\Omega\tau) \quad (22)$$

with $A(\tau)$ and $B(\tau)$ given by (20) and (21). It is straightforward to see that for $\beta \to 0$ and $\Omega \to 0$ we obtain $A(\tau) = a_0$ and $B(\tau) = -\tau/2$, i.e., the linear resonant case. For $T \to \infty$ the system reaches the steady solution

$$Q(T) \approx A(\tau)\cos(T+\Omega\tau) + B(\tau)\sin(T+\Omega\tau) = \frac{2f\Omega}{\beta^2+4\Omega^2}\cos(T+\Omega\tau) - \frac{\beta f}{\beta^2+4\Omega^2}\sin(T+\Omega\tau) = \frac{f}{\sqrt{\beta^2+4\Omega^2}}\cos(\omega_C t + \Omega\varepsilon t + \psi), \quad (23)$$

with

$$\psi = \arctan\left[\frac{\beta}{2\Omega}\right].$$

The numerical check is shown in Figs. (4), (5) where we plotted the solution (22) in the transient and stationary regime

respectively. Here, and for all the next figures, data are reported in arbitrary units (a. u.). We compared the analytical result and the numerical simulation performed with the software LTspice, as detailed in Sec. VII. The agreement is excellent. We stress that the nonlinearity did not destroy the primary resonance. On the contrary, as we will see in the next sections, it creates new resonances.

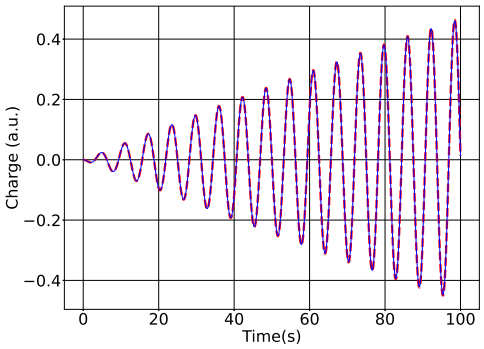

Fig. 4. Plot of the numerical (dotted line) and analytical (solid line) solution at primary resonance, $\omega_R = 1$, for $Q(T)$ given by Eq. (22) during the transient. The values of the other parameters are $\varepsilon = 0.01$, $\beta = 0.1$, $\Omega = 1$, $f = 1$.

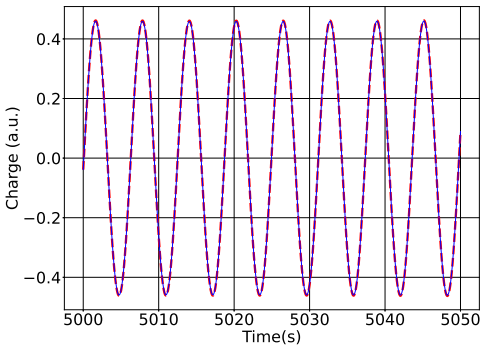

Fig. 5. Plot of the numerical (dotted line) and analytical (solid line) solution at primary resonance, $\omega_R = 1$, for $Q(T)$ given by Eq. (22) in the stationary regime. The values of the other parameters are $\varepsilon = 0.01$, $\beta = 0.1$, $\Omega = 1$, $f = 1$.

IV. Solution near the secondary resonances

We now consider the case far from the LC-resonance with a current not necessarily small, $i_1(t) = i_0 \sin \omega t$. First we seek for secondary resonances. To do that we study (11) with the standard approach (straightforward expansion) $Q = u_0(T) + \varepsilon u_1(T) + \cdots$, we have

$$\frac{\partial^2}{\partial T^2} u_0(T) + u_0(T) = -F \cos \omega_R T, \tag{24}$$

$$\frac{\partial^2}{\partial T^2} u_1(T) + u_1(T) = -\beta \frac{\partial}{\partial T} u_0(T) + u_0(T) \left(\frac{\partial}{\partial T} u_0(T) + \frac{F}{\omega_R} \sin \omega_R T \right), \tag{25}$$

with

$$\omega_R \equiv \frac{\omega}{\omega_C}, \; F \equiv \frac{i_0 \omega_R}{Q_0 \omega_C}.$$

The solution of (24) is

$$u_0(T) = c_1 \cos T + c_2 \sin T - \frac{F \cos \omega_R T}{1 - \omega_R^2} \tag{26}$$

Plugging (24) into (25) we may easily solve (25) using standard techniques. We do not write down the large expression of the solution for brevity. We limit ourselves to stress that, analyzing the solution, in addition to $\omega_R = 1$, we find secondary resonances at $\omega_R = 0, 1/2, 2$. The next step is to manipulate (11) in such a way to obtain an equation formally written as (1) so that we can apply the mathematical tools used in this paper, in particular, the Average Theorem [20]. To do that, we set

$$Q = U + Q_p = U - \frac{F \cos \omega_R T}{1 - \omega_R^2}, \tag{27}$$

where Q_p is the particular solution of (11) at zero-order ε. After a little algebra we end up into

$$\frac{d^2 U}{dT^2} + U = \varepsilon h \left(U, \frac{dU}{dT}, T \right) \tag{28}$$

with the nonlinear term $h\left(U, \frac{dU}{dT}, T\right)$ given by the expression

$$h\left(U, \frac{dU}{dT}, T\right) = -\beta \left[\frac{d}{dT} \left(-\frac{F \cos(\omega_R T)}{1 - \omega_R^2} \right) + \frac{dU}{dT} \right] + \left(U - \frac{F \cos(\omega_R T)}{1 - \omega_R^2} \right) \times \left[\frac{dU}{dT} + \frac{d}{dT} \left(-\frac{F \cos(\omega_R T)}{1 - \omega_R^2} \right) + \frac{F \sin(\omega_R T)}{\omega_R} \right]. \tag{29}$$

Following the approach of [20] we perform the transformation (van der Pol transformation)

$$\begin{bmatrix} u \\ v \end{bmatrix} = A \begin{bmatrix} U \\ \frac{dU}{dt} \end{bmatrix}, \tag{30}$$

$$A = \begin{bmatrix} \cos\left(\frac{\omega_R T}{k}\right) & -\frac{k}{\omega_R} \sin\left(\frac{\omega_R T}{k}\right) \\ -\sin\left(\frac{\omega_R T}{k}\right) & -\frac{k}{\omega_R} \cos\left(\frac{\omega_R T}{k}\right) \end{bmatrix} \tag{31}$$

and, inverting the transformation, we have

$$U = u \cos\left(\frac{\omega_R T}{k}\right) - v \sin\left(\frac{\omega_R T}{k}\right), \tag{32}$$

$$\frac{dU}{dt} = -\frac{\omega_R}{k} \left[u \sin\left(\frac{\omega_R T}{k}\right) + v \cos\left(\frac{\omega_R T}{k}\right) \right]. \tag{33}$$

Deriving (30) in which $U, \frac{dU}{dt}$ can be written as functions of u, v, t via (30) itself, and using (28) we finally get

$$\frac{du}{dT} = -\frac{k}{\omega_R} \left[\varepsilon h + \left(\frac{\omega_R^2 - k^2}{k^2} \right) U \right] \sin\left(\frac{\omega_R T}{k}\right), \tag{34}$$

$$\frac{dv}{dT} = -\frac{k}{\omega_R} \left[\varepsilon h + \left(\frac{\omega_R^2 - k^2}{k^2} \right) U \right] \cos\left(\frac{\omega_R T}{k}\right). \tag{35}$$

We are interested to the case $k^2-\omega_R^2=\varepsilon\Gamma$. We may rewrite (32) and (33) as

$$\frac{du}{dT}=-\varepsilon\frac{k}{\omega}\left[h-\left(\frac{\Gamma}{k^2}\right)U\right]\sin\left(\frac{\omega_R T}{k}\right), \quad (36)$$

$$\frac{dv}{dT}=-\varepsilon\frac{k}{\omega}\left[h-\left(\frac{\Gamma}{k^2}\right)U\right]\cos\left(\frac{\omega_R T}{k}\right). \quad (37)$$

We are now in the position to apply the Averaging Theorem [20]. In this case, it coincides with taking the average on the right-hand-side of (36) and (37) during the period corresponding to the frequency ω_R, keeping the functions u and v as constants while averaging. We are interested in two cases: $\omega_R\approx 1/2$ and $\omega_R\approx 2$, which will be studied in detail in the next sections.

V. Secondary resonance: $\omega_R\approx 2$

Substituting (32) and (33) into (36) and (37), we obtain two quite large expressions containing the functions u and v and trigonometric functions. Applying the Averaging Theorem [20] with $\omega_R=\sqrt{k^2-\varepsilon\Gamma}=\sqrt{4-\varepsilon\Gamma}$ we find

$$\frac{du}{dT}=-\varepsilon\left[\left(\frac{\beta}{2}+\frac{F}{24}\right)u(T)+\frac{1}{8}\Gamma v(T)\right], \quad (38)$$

$$\frac{dv}{dT}=-\varepsilon\left[\left(\frac{\beta}{2}-\frac{F}{24}\right)v(T)-\frac{1}{8}\Gamma u(T)\right]. \quad (39)$$

The above equations can be solved. As reference we write the approximated solution for $\omega_R\approx 2$ with initial conditions $Q(0)=0$, $Q'(0)=0$.

$$\begin{aligned}Q(T)\approx&-\frac{F\cos(\omega_R T)}{1-\omega_R^2}+\frac{F}{1-\omega_R^2}\times\\&\exp\left[-\frac{1}{2}\beta\varepsilon T\right]\cos\left[\frac{\varepsilon T}{24}\sqrt{9\Gamma^2-F^2}\right]\times\\&\left[\cos\left[\frac{\omega_R}{2}T\right]+\frac{\varepsilon(12\beta+F)\sin\left[\frac{\omega_R}{2}T\right]}{3\left(4\omega_R+\varepsilon\Gamma\right)}\right]-\\&\frac{F}{1-\omega_R^2}\exp\left[-\frac{1}{2}\beta\varepsilon T\right]\frac{\sin\left[\frac{\varepsilon T}{24}\sqrt{9\Gamma^2-F^2}\right]}{\sqrt{9\Gamma^2-F^2}}\times\\&\left[\frac{\left(36\Gamma\omega_R-\varepsilon\left(-9\Gamma^2+F^2+12\beta F\right)\right)\sin\left[\frac{\omega_R}{2}T\right]}{3\left(\Gamma\varepsilon+4\omega_R\right)}+\right.\\&\left.\frac{4\left(F\omega_R-3\beta\Gamma\epsilon\right)\cos\left[\frac{\omega_R}{2}T\right]}{\Gamma\varepsilon+4\omega_R}\right], \end{aligned} \quad (40)$$

with $\omega_R=\sqrt{k^2-\varepsilon\Gamma}=\sqrt{4-\varepsilon\Gamma}$. We stress that although we studied an approximation of (9), i.e., (11), the analytical results, in the range of the parameters keeping finite the solution, are in excellent agreement with the numerical solution of the exact equation (see Fig. 6). Seeking the range of the parameters that generates an exponential growing solution, we may limit ourselves to analyzing the system's eigenvalues. We find that when $\omega_R\approx 2$

$$\lambda_1=\frac{\varepsilon}{24}\left(-12\beta-\sqrt{F^2-9\Gamma^2}\right), \quad (41)$$

$$\lambda_2=\frac{\varepsilon}{24}\left(-12\beta+\sqrt{F^2-9\Gamma^2}\right). \quad (42)$$

We infer that the parameter region corresponding to an exponential growing solution can be determined by imposing $\lambda_2>0$, that is

$$F^2\geq 144\beta^2+9\Gamma^2,\ \ \Gamma\leq\frac{F}{3} \quad (43)$$

The divergence of the solution in the parameter range given by (43) has to be attributed to the approximation used for the analytical study of (9), namely the use of (11). We finally observe that, although the resonance $\omega_R=2$ does not cause a considerable increase in the amplitude of the signal, the system exhibits a negative μ as numerically shown in the Sec. VII.

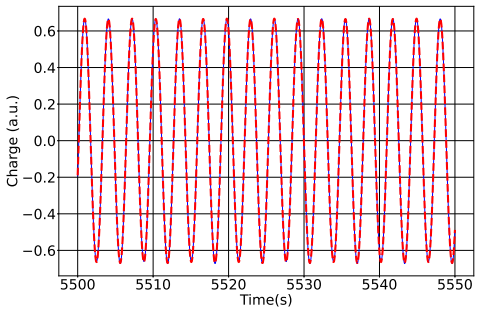

Fig. 6. Plot of numerical (dashed line) and analytical expression (solid line) for $Q(T)$ given by Eq. (40), in the stationary regime. The values of the parameters are $\beta=0.1$, $\varepsilon=0.01$, $\omega_R=2$, $F=1$, $\Gamma=0$. The two curves are indistinguishable.

VI. Secondary resonance: $\omega_R\approx 1/2$

As done in the previous section, following again [20], we may repeat the same calculations for $\omega_R=\sqrt{k^2-\varepsilon\Gamma}=\sqrt{1/4-\varepsilon\Gamma}$. We find the following system of differential equations

$$\frac{du}{dT}=-\varepsilon\left[\frac{\beta\omega_R}{2}u+\Gamma v-\frac{F^2}{8\omega_R^2\left(1-\omega_R^2\right)^2}\right], \quad (44)$$

$$\frac{dv}{dT}=-\varepsilon\left[-\frac{\Gamma}{\omega_R}u+\frac{\beta}{2}v\right]. \quad (45)$$

The system is linear and its solution, with initial conditions $Q(0)=0$, $Q'(0)=0$, is

$$\begin{aligned}Q(T)\approx&\frac{F^2\left[\beta\omega_R\cos\left(\frac{T\omega_R}{k}\right)-2\Gamma\sin\left(\frac{T\omega_R}{k}\right)\right]}{4\left(1-\omega_R^2\right)^2\omega_R\left(\beta^2\omega_R^2+4\Gamma^2\right)}-\\&\frac{F\cos(T\omega_R)}{1-\omega_R^2}-F\exp\left[-\frac{1}{2}\beta\tau\right]\cos\left[\frac{T\omega_R}{k}+\frac{\tau\Gamma}{\omega_R}\right]\\&\frac{\beta F-4\left(1-\omega_R^2\right)\left(\beta^2\omega_R^2+4\Gamma^2\right)}{4\left(1-\omega_R^2\right)^2\left(\beta^2\omega_R^2+4\Gamma^2\right)}+\\&\exp\left[-\frac{1}{2}\beta\tau\right]F\omega_R\sin\left[\frac{T\omega_R}{k}+\frac{\tau\Gamma}{\omega_R}\right]\\&\frac{\beta\varepsilon k\left[4\left(1-\omega_R^2\right)\left(\beta^2\omega_R^2+4\Gamma^2\right)-\beta F\right]+4F\Gamma}{8\left(1-\omega_R^2\right)^2\left(\beta^2\omega_R^2+4\Gamma^2\right)\left(\varepsilon k\Gamma+\omega_R^2\right)}. \end{aligned} \quad (46)$$

Figs. 7 and 8 show a very good agreement between analytical and numerical checks. We note that the resonance $\omega_R = 1/2$ causes a considerable increase in the signal's amplitude but without the divergence characteristic of the primary resonance. Thus if we do not exit from the Rayleigh zone, our results remain valid.

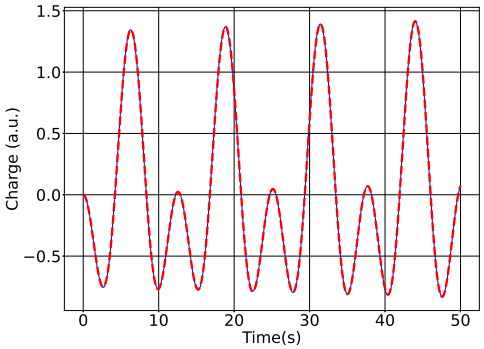

Fig. 7. Plot of numerical (dashed line) and analytical expression (solid line) for $Q(T)$ given by (46) in transient regime. The values of the parameters are $\beta = 0.1,\ \varepsilon = 0.01,\ \omega = 1/2,\ F = 1,\ \Gamma = 0$.

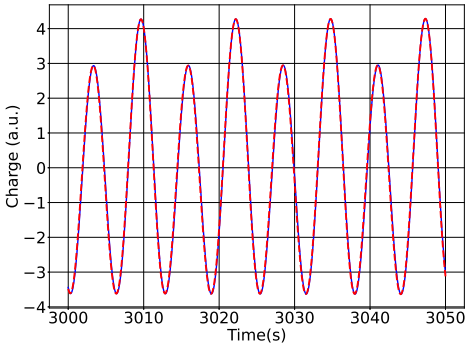

Fig. 8. Plot of numerical (dashed line) and analytical expression (solid line) for $Q(T)$ given by (46) in stationary regime. The values of the parameters are $\beta = 0.1,\ \varepsilon = 0.01,\ \omega = 1/2,\ F = 1,\ \Gamma = 0$.

VII. Numerical Analysis

In Fig. 9, we show the circuit model adopted to derive the numerical results compared with the analytical calculations of Secs. III–VI. Simulations are performed with the LTspice software environment.

The electric circuit of Fig. 3 shows a current generator i_1 driving a primary inductance L_1 magnetically coupled to a constant inductance L_0, which is in turn connected in series to a dependent voltage source B, a resistance R and a capacitance C. To numerically match with the analytical study, we fixed $L_0 = 1$ H, the mutual inductance between L_1 and L_0 equal to 1 H, $R = 1\ \Omega$, and $C = 1$ F. More specifically, the element B is an LTspice behavioral voltage source, and it is adopted to implement the discussed nonlinearity, according to (5).

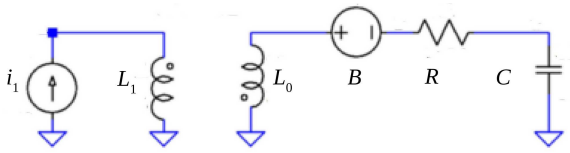

Fig. 9. Spice circuit.

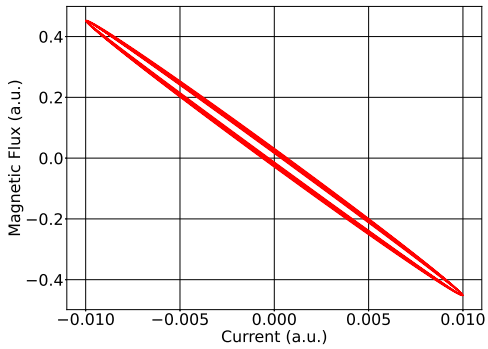

Fig. 10. Flux versus current at the primary resonance at $\omega_R = 1$. The values of the other parameters are $\varepsilon = 0.01$, $\beta = 0.1$.

As shown in Figs. 4–8, the comparison between the numerical and analytical solutions is excellent.

We now focus on the magnetic properties of the system. The total flux, i.e., the flux through the external solenoid, is (initial conditions $Q(0) = 0,\ Q'(0) = 0$

$$\Phi_T = L^* i_1(T) - RQ - \frac{1}{C}\int_0^T Q(u)du \qquad (47)$$

which is the sum of the flux through the resonator, i.e., $-RQ - 1/C\int_0^T Q(u)du$, and the flux through the circular crown between the external solenoid and the resonator, i.e., $L^* i_1(T)$. Therefore, $L^* = L_{wo-res}(1 - \pi r_{res}^2/a^2)$, is the circular crown self-inductance, and L_{wo-res} is the self-inductance of the unit-cell without the resonator. Finally, r_{res} is the resonator radius.

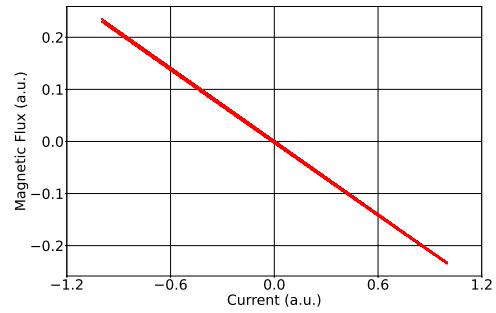

Fig. 11. Flux versus current at the secondary resonance at $\omega_R = 2$. The values of the other parameters are $\varepsilon = 0.01$, $\beta = 0.1$.

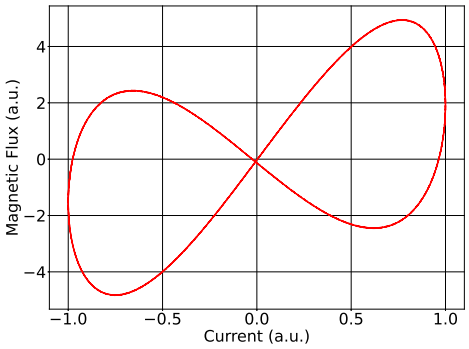

Fig. 12. Flux versus current at the secondary resonance at $\omega_R = 1/2$. The values of the other parameters are $\varepsilon = 0.01$, $\beta = 0.1$.

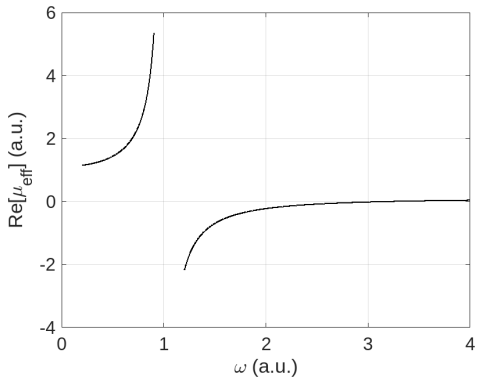

Fig. 13. Plot of the real part of $\mu_{\rm eff}$ versus the dimensionless frequency ω. Results are analytically derived from (49)-(53); $\omega = 1$ refers to the primary resonance.

Let us now consider the case $t \to \infty$ at which the system works in a steady-state. The results for the primary resonance, $\omega_R = 1$, are summarized in Fig. (10) and, for the secondary resonances, in Figs. (11), and (12), for $\omega_R = 2, 1/2$ respectively.

Effective Magnetic Permeability $\mu_{\rm eff}(\omega)$ With phasor notation, let us now analyze the sign of the effective permeability $\mu_{\rm eff}$ [5]

$$\mu_{\rm eff}(\omega) = \frac{B_{\rm ave-iso}(\omega)}{\mu_0 H_{\rm ave}(\omega)} \propto \frac{\Phi_{T-iso}}{I_1} \tag{48}$$

where $B_{\rm ave-iso}$ and $H_{\rm ave}$ still refer to the spatial averages as defined in Fig. 2, and, furthermore, $B_{\rm ave-iso}$ ($\Phi_{\rm T-iso}$), takes into account the only isofrequency component of the magnetic flux density (magnetic flux) with the driven sinusoidal magnetic field (driven current I_1).

Then for frequencies sufficiently far from 1, from (40) and (47) we have for the magnetic flux:

$$\Phi_T = -\frac{\varepsilon\beta F\cos(\omega T)}{\omega^2-1} + \frac{F}{\omega}\left[L^* - \frac{1}{C(\omega^2-1)}\right]\sin(\omega T) = \rho\sin(\omega T+\phi) \tag{49}$$

where we choose $i_1(T) = F\sin(\omega T)/\omega$ so to obtain the first term on the right hand side of (24) and, by definition:

$$\rho = \frac{F}{\omega}\sqrt{\left(L^* - \frac{1}{C(\omega^2-1)}\right)^2 + \left(\frac{\varepsilon\beta\omega}{\omega^2-1}\right)^2} \tag{50}$$

$$\sin\phi = -\frac{\varepsilon\beta F}{\rho(\omega^2-1)}, \tag{51}$$

$$\cos\phi = \left(L^* - \frac{1}{C(\omega^2-1)}\right)\frac{F}{\omega\rho}. \tag{52}$$

For $|\mu_{\rm eff}(\omega)|$ we obtain:

$$|\mu_{\rm eff}(\omega)| \propto \sqrt{\left(L^* - \frac{1}{C(\omega^2-1)}\right)^2 + \left(\frac{\varepsilon\beta\omega}{\omega^2-1}\right)^2} \tag{53}$$

We can finally analyze the sign of the real part of $\mu_{\rm eff}(\omega)$ as reported in Figs. 13.

In particular, we can observe how the real part of the effective permeability becomes negative from the primary resonance to about three times its value, thus showing a wider frequency range with respect to the air-core linear case as discussed in [5] and [6], for which the frequency range over which we can get negative values of the effective permeability is very limited close around the frequency resonance.

The presence of magnetic material with $\mu_r \sim 10^2$ can reduce the cell dimensions for a required resonance frequency or, alternatively, diminish the resonance frequency if the cell dimensions are maintained. However, the observed amplitude resonance at $\omega = 1/2$ has to be properly considered to avoid possible undesired overvoltages on the circuit elements.

VIII. Conclusion

We investigated the behavior of a metamaterial made of nonlinear magnetic core filled-resonators, with the core operating in the Rayleigh region. The study was performed by deriving a nonlinear circuit model and adopting perturbative analytical approaches for the solution. As a significant result, we showed that the nonlinear filling material determines secondary resonances at one-half and twice the primary resonance. In particular, the input field is significantly amplified at one-half the primary resonance. At the same time, the real part of the effective magnetic permeability maintains a positive value around such a frequency range. On the other hand, at twice the primary resonance, the input signal amplitude practically maintains unchanged, while the effective permeability is still negative. Indeed, the effective permeability gets negative values from the primary resonance up to about three times its value, and it substantially shows a linear behavior for frequencies larger than the primary resonance. We performed a numerical analysis with a circuit simulator, and it validated the analytical results with a very good agreement. Finally, the use of magnetic cores allows for reducing the cell dimensions for a given primary resonance frequency, as well as for extending the application up to industrial frequencies, and for reaching larger negative values of the real part of the effective magnetic permeability. However, the secondary resonance at one-half

the primary resonance has to be properly taken into account for an accurate design of the metamaterial.

ACKNOWLEDGMENT

K.J.C. and M.B. acknowledge financial support from UTA Mayor project No 8737-22.

REFERENCES

[1] J. B. Pendry, A. J. Holden, D. J. Robbins, and W. J. Stewart, "Magnetism from conductors and enhanced nonlinear phenomena," *IEEE Trans. Microw. Theory Tech.*, vol. 47, no. 11, Nov. 1999, pp. 2075-2084.

[2] J. B. Pendry, A. J. Holden, W. J. Stewart, and I. Youngs, "Extremely low frequency plasmons in metallic mesostructures," *Phys. Rev. Lett.*, vol. 76, no. 25, Jun. 1996, pp. 4773-4776.

[3] B. J. Justice, J. J. Mock, L. Guo, A. Degiron, D. Schurig, and D. R. Smith, "Spatial mapping of the internal and external electromagnetic fields of negative index metamaterials," *Opt. Exp.*, vol. 14, no. 19, Sep. 2006, pp. 8694-8705.

[4] D. R. Smith and N. Kroll, "Negative refractive index in left-handed materials," *Phys Rev. Lett.*, vol. 85, no. 14, Oct. 2000, pp. 2933-2936.

[5] B. Tellini, M. Bologna and Alessandra Petri, "Measurement of Magnetism in Composite Materials," *IEEE Trans. Instr. Measur.*, vol. 58, no. 10, Sep. 2009, pp. 3411-3417.

[6] M. Bologna, A. Petri, B. Tellini, and C. Zappacosta, "Effective Magnetic Permeability Measurement in Composite Resonator Structures," *IEEE Trans. Instrum. Meas.*, vol. 59, no. 5, May 2010, pp. 1200-1206.

[7] B. Tellini and M. Bologna, "Magnetic Composite Materials and Arbitrary $B - H$ Relationships," *IEEE Trans. Magn.*, vol. 46, no. 12, Dec. 2010, pp. 3967-3972.

[8] C. Lu, X. Huang, C. Rong, X. Tao, Y. Zeng, and M. Liu, "A Dual-Band Negative Permeability and Near-Zero Permeability Metamaterials for Wireless Power Transfer System," *IEEE Trans. Ind. Electr.*, vol. 68, no. 8, Aug. 2021, pp. 7072-7082.

[9] S. T. S. Udayanga, N. Kularatna, and D. A. Steyn-Ross, "Investigating the impact of ferrite magnetic cores on the performance of supercapacitor assisted surge absorber (SCASA) technique," IEEE 28th International Symposium on Industrial Electronics (ISIE), 2019, pp. 130-139.

[10] C. C. M. Carmo, R. M. S. Batalha, L. D. Ribeiro, and Ú. C. Resende, "Metamaterial Based Broadband Absorber Design," *IEEE Trans. Magn.*, vol. 58, no. 2, Feb. 2022, pp. 2500405(1-5).

[11] G. Lipworth, J. Ensworth, K. Seetharam, J. S. Lee, P. Schmalenberg, T. Nomura, M. S. Reynolds, D. R. Smith, Y. Urzhumov, "Quasi-Static Magnetic Field Shielding Using Longitudinal Mu-Near-Zero Metamaterials," *Scientific Reports*, 5, 12764, 2015, pp. 1-8.

[12] H. Wang, W. Wang, X. Chen, Q. Li, Z. Zhang, "Analysis and Design of kHz-Metamaterial for Wireless Power Transfer," *IEEE Trans. Magn.*, vol. 56, no. 8, Aug. 2020, pp. 6703215(1-5).

[13] Y. Urzhumov, W. Chen, C. Bingham, E. Padilla, D. R. Smith, "Magnetic levitation of metamaterial bodies enhanced with magnetostatic surface resonances," *Phys. Rev. B*, vol. 85, 2012, 054430(1-12).

[14] L. M. Holmes, "Stability of magnetic levitation," *J. Appl. Phys.*, vol. 49, 1978, pp. 3102-3109.

[15] I. V. Shadrivov, A. A. Zharov, N. A. Zharova, Y. S. Kivshar, "Nonlinear left-handed metamaterials," *Radio Sci.*, vol. 40, May 2005, pp. RS3S90(1-10).

[16] M. Lapine, I. V. Shadrivov, Y. S. Kivshar, "Colloquium: Nonlinear metamaterials," *Rev. Mod. Phys.*, vol. 86, Sept. 2014, pp. 1093(1-26).

[17] P. Porfyrakis, N. L. Tsitsas, "Nonlinear electromagnetic metamaterials: Aspects on mathematical modeling and physical phenomena," *Microelectronic Engineering*, vol. 216, Aug. 2019, pp. 111028(1-10).

[18] M. Osinalde, P. Infante, L. Domínguez, J. M. Blanco, A. Chizhik, V. Zhukova, A. Zhukov, and J. González, "Magnetic Characterization in the Rayleigh Region of Nanocrystalline Magnetic Cores," *Materials*, vol. 11, Nov. 2018, pp. 2278-2284.

[19] J. Kevorkian, J. D. Cole, *Multiple Scale and Singular Perturbation Methods*, Springer-Verlag, NewYork 1996.

[20] J. Guckenheimer, P. Holmes, *Nonlinear Oscillations, Dynamical Systems, and Bifurcations of Vector Fields*, Springer, 2002.

[21] M. Kachniarz, R. Szewczyk, "Study on the Rayleigh Hysteresis Model and its Applicability in Modeling Magnetic Hysteresis Phenomenon in Ferromagnetic Materials," *Acta Physica Polonica Series a*, vol. 131, May 2017, pp. 1244-1249.

Mauro Bologna was born in 1961. He received the M.Sc. (Laurea) degree in physics from the University of Pisa, Pisa, Italy, in 1988, and the Ph.D. degree in physics from the University of North Texas, Denton, TX, USA, in 2002. From 1999 to 2003, he was with the Center of Nonlinear Science, University of North Texas. He is currently a Professor with the Department of Electrical and Electronic Engineering, Universidad de Tarapacá, Arica, Chile. His main research fields are non-Poissonian processes, magnetohydrodynamics, and nonlinear science.

Kristopher J. Chandía (Member, IEEE) was born in Arica, Chile, in 1979. He received the B.S. degree in electronic engineering, the M.S. degree in telecommunications engineering, and the Ph.D. degree in science from the Universidad de Tarapacá, Arica, in 2005, 2006, and 2010, respectively. Since 2010, he has been with the Universidad de Tarapacá, where he is currently an Assistant Professor with the Department of Electrical and Electronic Engineering. His research activities include nonlinear circuits, memristors, electromagnetic wave theory, waveguides, and optical fibers in communication systems. Dr. Chandía has been the Editor-in-Chief of Ingeniare Revista Chilena de Ingeniería since 2012.

Bernardo Tellini (Senior Member, IEEE) was born in Pisa, Italy, in 1969. He received the M.S. (Laurea) and Ph.D. degrees in electrical engineering from the University of Pisa, Pisa, in 1993 and 1999, respectively. Since 2000, he has been with the University of Pisa, where he is currently a Full Professor of electrical measurements with the Department of Energy, Systems, Territory and Construction Engineering. His research interests include electrical and magnetic materials, aging process in battery cells, pulsed power applications and fast electromagnetic transients, magnetohydrodynamics. Prof. Tellini is a member of the IEEE Instrumentation and Measurement Society and the IEEE Magnetics Society. He was the Chair of the European Pulsed Power Laboratories from 2010 to 2014. He has served as the general chair and the general co-chair for several IEEE conferences. He was the Chair of the IEEE Italy Section (2019-2021).